



Effect of $\text{Ba}(\text{Zn}_{1/3}\text{Nb}_{2/3})\text{O}_3$ modification on structure and ferroelectric properties of $0.6\text{Pb}(\text{Mg}_{1/3}\text{Nb}_{2/3})\text{O}_3-0.4\text{Pb}(\text{Zr}_{0.52}\text{Ti}_{0.48})\text{O}_3$ ceramics

Hassakorn Wattanasarn^a, Wattana Photankham^a, Tosawat Seetawan^{a,*}, Rattikorn Yimnirun^b, Chanchana Thanachayanont^c

^aThermoelectrics Research Center, Research and Development Institute, and Program of Physics, Faculty of Science and Technology, Sakon Nakhon Rajabhat University, 680 Nittayo Road, Sakon Nakhon 47000, Thailand

^bSchool of Physics, Institute of Science, and COE-NANOTEC-SUT on Advanced Functional Nanomaterials, Suranaree University of Technology, Nakhon Ratchasima 30000, Thailand

^cNational Metal and Materials Technology Center, National Science and Technology Development Agency, 114 Thailand Science Park, Phahonyothin Road, Klong 1, Klong Luang, Pathumthani 12120, Thailand

Received 27 January 2015; accepted 5 March 2015

Available online 11 March 2015

Abstract

In this study, $(1-x)[0.6\text{Pb}(\text{Mg}_{1/3}\text{Nb}_{2/3})\text{O}_3-0.4\text{Pb}(\text{Zr}_{0.52}\text{Ti}_{0.48})\text{O}_3]-x\text{Ba}(\text{Zn}_{1/3}\text{Nb}_{2/3})\text{O}_3$; $(1-x)\text{PMNZT60/40}-x\text{BZN}$ having $x=0, 2.5, 5, 7.5$, and 10 mol% ceramics were prepared by mixed oxide powder method and sintered using a two-step process. Phase transitions were investigated by XRD, microstructure by SEM, crystal morphology by TEM, the dielectric and ferroelectric properties by capacitance measurement setup and modified Sawyer-Tower circuit, respectively. The dielectric constant and dielectric loss tangent were measured as functions of both temperature and frequency. The XRD results show the phase transition from tetragonal phase to pseudo-cubic phase with addition of BZN in PMNZT system. Grain size of about 1.23–2.42 μm and crystallite size in a range of 421–2152 nm were obtained. The pure-phase 0.6PMN–0.4PZT ceramics show the normal ferroelectric behavior. The 0.95(PMNZT60/40)–0.05BZN and 0.925(PMNZT60/40)–0.075BZN showed a broad and diffused dielectric properties and the dispersive phase transition, indicating the relaxor ferroelectric behavior. The transition temperature in the BZN-modified PMNZT system is seen to decrease from 166 °C in pure PMNZT60/40 to 102 °C and 54 °C with increasing BZN content to 5 and 10 mol%, respectively. In addition, the maximum dielectric constant is decreased with increasing BZN content. The $P-E$ hysteresis loop measurements show the change from the normal ferroelectric behavior in PMNZT60/40 ceramic to more relaxor behavior that was induced with BZN addition. These results clearly demonstrated the significance of BZN to the electrical responses of the PMNZT60/40 system.

© 2015 Elsevier Ltd and Techna Group S.r.l. All rights reserved.

Keywords: Dielectric properties; Ferroelectric properties; Microstructure; Hysteresis loop; PMNZT

1. Introduction

Ferroelectric materials are promising candidates for portable microelectronic applications such as a self-sustained energy-harvesting battery charger. $\text{Pb}(\text{Mg}_{1/3}\text{Nb}_{2/3})\text{O}_3$ (PMN) ceramic is one of ferroelectric materials which exhibits linear electrostrictive and high dielectric properties [1–4], with vanished hysteresis loop behavior and pyrochlore phase easily appeared in the sintering process because PbO is evaporated at temperature

range of 870 °C. The $\text{Pb}(\text{Zr}_{0.52}\text{Ti}_{0.48})\text{O}_3$ (PZT) ceramic is one of the piezoelectric ceramics which have been investigated extensively, because of its excellent dielectric and polarization properties. It has non-linear electrostrictive properties, good dielectric and piezoelectric properties at low temperatures [5,6]. Both normal ferroelectric PZT and relaxor ferroelectric PMN are expected to combine the properties of which $\text{Pb}(\text{Mg}_{1/3}\text{Nb}_{2/3})\text{O}_3-\text{Pb}(\text{Zr}_{0.52}\text{Ti}_{0.48})\text{O}_3$ (PMNZT) could improve piezoelectric and dielectric properties from the single system of either PZT or PMN [7–9]. Cubic pyrochlore phase exists in PMN ceramics prepared by conventional mixed oxide method and the columbite precursor [10,11] that exhibits low dielectric constants. For the

*Corresponding author.

E-mail address: tseetawan@yahoo.com (T. Seetawan).

PMNZT system in which oxides were mixed together, previous works have only focused on 0.6PMN–0.4PZT (PMNZT60/40) which is one of the materials consisting of morphotropic phase boundary (MPB) [12–15]. There has been studies on the dielectric and ferroelectric properties of the ceramics within the entire compositional ranges near MPB [16,17]. But their temperature stability and reproducibility are required to be improved due to fast reduction of the dielectric constant at lower and higher temperatures than the Curie temperature introducing a narrow range for application. Meanwhile, $\text{Ba}(\text{Zn}_{1/3}\text{Nb}_{2/3})\text{O}_3$ (BZN) is one of the candidates for microwave dielectric materials that have been employed as resonators and filters for wireless communication technologies because of their high permittivity and low dielectric losses in the wavelength of micro and millimeter [18].

Therefore, as an extension to the prior research on the PMNZT60/40 ceramics, the main purpose of this study is to examine that BZN addition should be an aid for the improvement of the dielectric properties of PMNZT60/40 ceramics by slowing down the decrease of the dielectric constant above the Curie temperature. Therefore, the temperature and frequency dependence of the dielectric properties and the ferroelectric behaviors of ceramics in the $(1-x)[0.6\text{Pb}(\text{Mg}_{1/3}\text{Nb}_{2/3})\text{O}_3-0.4\text{Pb}(\text{Zr}_{0.52}\text{Ti}_{0.48})\text{O}_3]-x\text{Ba}(\text{Zn}_{1/3}\text{Nb}_{2/3})\text{O}_3$; $(1-x)\text{PMNZT60/40}-xBZN$ where $x=0, 2.5, 5, 7.5, \text{ and } 10$ mol% ternary system prepared by a conventional mixed oxide method were investigated in this study.

2. Experiment

The PMNZT 60/40 ceramics used in this study were prepared by mixed oxide method. The PMN were obtained by the columbite method. Firstly, magnesium niobate (MgNb_2O_6 ; MN) precursors were prepared from the stoichiometric ratio of raw materials of a high purity MgO (98%) with 3 mol% excess, and Nb_2O_5 (99.9%) mixed with ball-milling, fired at 1000°C for 6 h. Secondly, ZnO (99%), Nb_2O_5 and BaCO_3 (99%) powders were mixed in ball-milling and then fired 1100°C for 6 h to form barium zinc niobate [$\text{Ba}(\text{Zn}_{1/3}\text{Nb}_{2/3})\text{O}_3$; BZN]. PMNZT–BZN were prepared by solid state reaction of reagent grade MN, PbO (99%) excess with 4 mol% for compensated PbO volatilization during heat treatment, ZrO_2 (99%), TiO_2 (98%) and BZN. These powders were ball-milled for 24 h in deionize water, and then vaporized by hotplate. The mixed powder was pressed using two step sintering process [19]. Then, the sample was treated in PbO atmosphere by covering the sample with PZT powder in an alumina crucible, heated to 850°C with the heating rate of $10^\circ\text{C}/\text{min}$ and then soaked in that temperature for 4 h and cooled down at room temperature. The sample was crushed into powder and mixed with an aqueous solution (5 wt%) of polyvinyl alcohol and pressed into pellets at 190 MPa in disc shape with diameter 20 mm and 1.8 mm for thickness. Secondly, the samples were sintered at 1100°C for 2 h with the heating rate of $10^\circ\text{C}/\text{min}$, mixed oxide preparing process diagram, as seen in Fig. 1. In order to maintain lead atmosphere during the firing process, sample pellets were embedded in the PZT powder that came from the first step. After

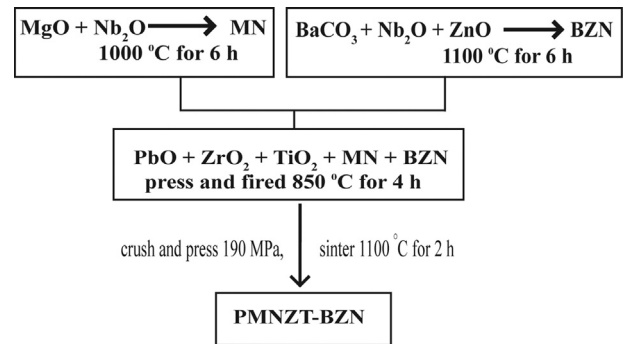


Fig. 1. Mixed oxide preparing diagram of PMNZT–BZN ceramics.

sintering, the sintered samples were polished to remove the lead rich layer on the samples.

The phase formation of powder and sintered samples were studied with an X-ray diffractometer (Shimadzu XRD–6100). The XRD patterns were recorded at room temperature with $\text{Cu K}\alpha_1$ radiation. Diffraction intensity was measured 2θ between 20° and 70° with step up 0.02° . Density of the sintered ceramics was measured by the Archimedes method. Microstructure characterization was carried out on the fractured surfaces of specimens using Scanning Electron Microscopy (SEM: JEOL Model JSM-5410). Grain sizes of sintered samples were estimated by a linear intercept method from SEM micrographs. Crystallite sizes were estimated from Transmission electron microscopy (TEM) images and selected area electron diffraction (SAED) were performed using a JEOL JEM-2010 transmission electron microscope operated at an accelerating voltage of 200 kV. The samples were coated with silver paint on the sample surfaces as electrode for dielectric measurements. The capacitances were obtained using a GW INSTEK LCR-821 connected to the sample electrode surfaces. The sample with probe were immersed in silicon oil bath and then heated at room temperature to 200°C . In this study, the dielectric constants were measured at a discrete frequency range of 1–100 kHz. The capacitances were used to determine the dielectric constants as follow $\epsilon_r = Ct/\epsilon_0A$; where C is the capacitance of the sample, t and A are the thickness and the area of the electrode, respectively, and ϵ_0 is the dielectric permittivity in vacuum (0.08854 pF/m). The ferroelectric hysteresis loops were characterized by using high voltage AC amplifier (Trek, model 20/20 C), the samples applied with 10 kV/cm and connected with Sawyer–Tower circuit and computer interfaces.

3. Results and discussion

3.1. Powder characteristics studies

The XRD patterns of $(1-x)\text{PMNZT60/40}-xBZN$ ($x=0, 2.5, 5, 7.5$ and 10 mol%) samples are shown in Fig. 2. All samples were sintered at 1100°C for 2 h. The patterns present the characteristics of complex perovskite cubic $(\text{A}(\text{B}'\text{B}'')\text{O}_3)$. In Fig. 2(a), PMNZT60/40 exhibited a tetragonal phase which is nearly at the morphotropic phase boundary (MPB) composition. BZN contents were gradually increasingly added into PMNZT60/

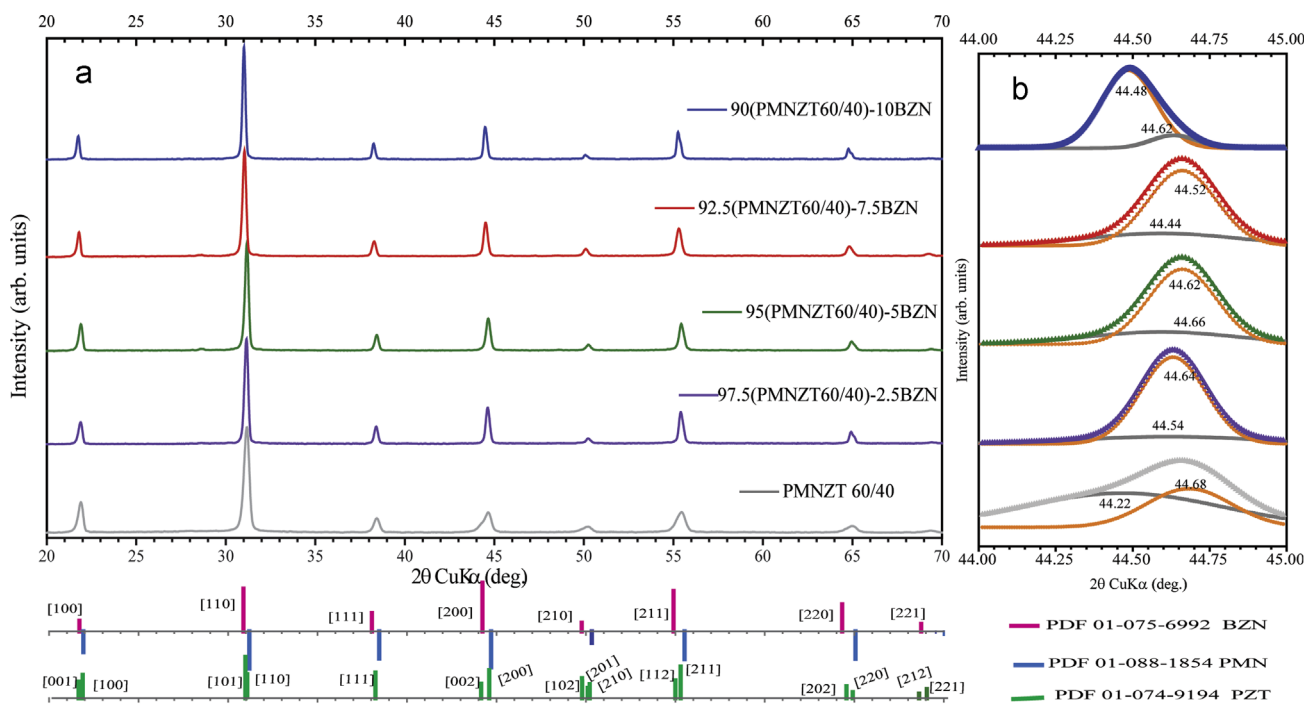


Fig. 2. (a) XRD patterns of $(1-x)$ PMNzT60/40- x BzN ($x=0, 2.5, 5, 7.5$ and 10 mol%) ceramics, (b) the inset shows the $[200]$ reflections around $2\theta=44-45^\circ$.

40, resulting in the changes in the degree 2θ peak that were slightly shifted to the left hand, implying the decreases of lattice parameter due to lattice strain and successful B' substitution to the B'' sites (1:2 order structure) [20]. Thus, the phase transformation from the tetragonal to the pseudo-cubic phase occurs with increasing BZN content. Using 2θ data from 20° to 70° of the XRD results, lattice parameters a , c and relative theoretical density are determined and shown in Table 1. The XRD pattern main differences are analyzed on the peaks of $[200]$ plane at nearly 45° because the $[200]$ plane is a single peak for the cubic and rhombohedral phase [21]. On the other hand, the tetragonal phase splits into two peaks at this peak. In order to determine the phase transition of various samples accurately, the board peak of $[200]$ plane lines of five samples obtained by an extraction from XRD pattern range $44^\circ-45^\circ$ are presented in Fig. 2(b). Gaussian peaks (dotted lines) were fitted with two curves on the $[200]$ reflections split to $[002]T$ and $[200]T$ which are in tetragonal phase of PMNzT60/40. It should be noted that the samples peak which shifted from left to right of the patterns, with gradually increasing BZN content, the integrated intensities of $[002]T$ decrease while the intensities of $[200]T$ shifted to $[200]C$, as observed in Fig. 2(b). For the MPB, the coexistence between the tetragonal and cubic phases of equal quantities is well known [22,23]. Consequently, increasing BZN content into PMNzT60/40 should result in the non-MPB compositions. However, from the $[200]$ reflections of 10 mol% BZN it was found that the $[002]T$ splits to 44.8° and 44.62° , suggesting that there is a phase transition to tetragonal structure when increasing BZN content more than 10 mol%.

Fig. 3 reveals that the mixed oxide powder consists of agglomerated nanoparticles. The crystallite shape is polygon for PMNzT60/40, as shown in Fig. 3(a). Meanwhile, adding BZN

Table 1

Density, theoretical density, lattice parameters a and c . Rietveld refinement using data from 20° to 70° of the XRD results in Fig. 2. Crystallite sizes obtained from TEM.

	Density (g/cm ³)	TD (%)	a (Å)	c (Å)	Crystal size (nm)	Average grain size (μm)
PMNzT 60/40	7.76	97.63	4.062	4.123	421	1.23
0.975PMNzT60/ 40-0.025BzN	7.67	95.67	4.060	4.071	814	1.56
0.95PMNzT60/ 40-0.05BzN	7.66	94.26	4.034	4.050	886	2.42
0.925PMNzT60/ 40-0.075BzN	7.71	96.45	4.049	4.068	1282	2.19
0.9PMNzT60/ 40-0.1BzN	7.49	94.54	4.056	4.075	2152	2

into PMNzT60/40 changes the crystallite shape of PMNzT60/40 to a long curved shape and larger size. Moreover, stacking faults are observed in the samples (white arrow,) as shown in Fig. 3(a-d). This suggests that the increased atomic species make it difficult for the crystalline materials to arrange the constituent atoms into ordered structure [24]. The formation processes of nanoscale oxide particles of $(1-x)$ PMNzT60/40- x BzN and also the amorphous structure follow the sequence: ordered structure \rightarrow disordered structure (loss of long-range order) \rightarrow fine grained (nanocrystalline) structure \rightarrow amorphous structure [25,26].

The SAED patterns of $(1-x)$ PMNzT60/40- x BzN ceramics are illustrated in Fig. 3 (insets), the diffraction rings of well-defined bright spots are typical diffraction patterns of polycrystalline materials. The interplanar distances (obtained from radius of the

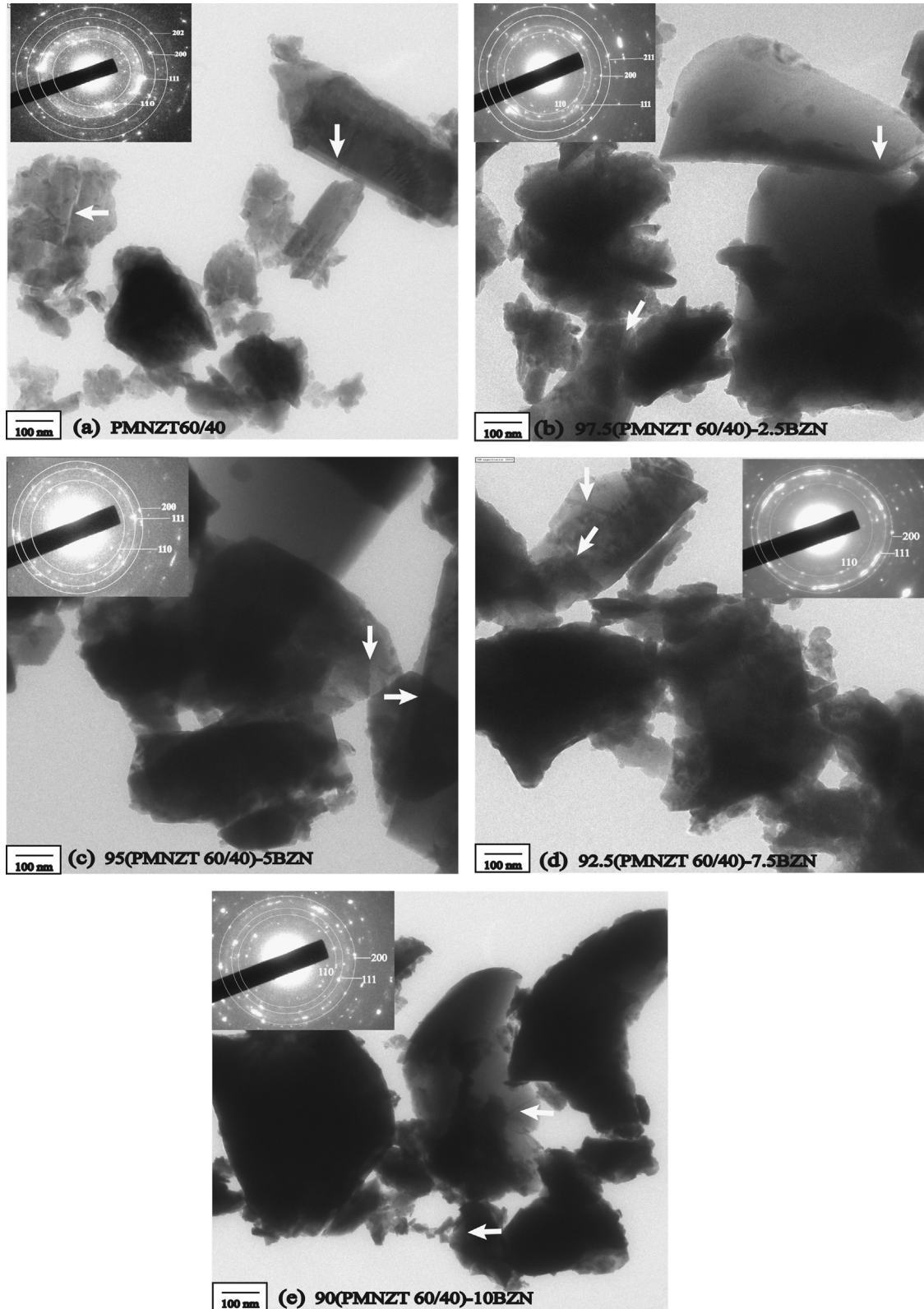


Fig. 3. Typical TEM micrographs with the corresponding selected area electron diffraction (SAED) patterns (insets) and Stacking faults (white arrow) of $(1-x)$ PMNzT60/40- x BzN ceramics synthesized by mixed oxide method, (a) 2.5, (b) 5 (c) 7.5, and (d) 10 mol%.

rings) correspond to the d -spacing of $(1-x)$ PMNzT60/40- x BzN ceramics. The results match well with those from the XRD patterns. In the SAED of PMNzT60/40 (inset in Fig. 3(a)), circular rings

were drawn passing bright spots indicating tetragonal crystal. In addition, the transmitted beam intensity was transferred to the scattered to the diffracted electron beams, and led to a diffraction

maximum at this same extinction thickness, thus conserving the total energy in the diffracted and direct transmitted beams that exit the sample [27]. The spot dispersion decreases with increasing BZN contents in PMNZT60/40 (see inset in Fig. 3(b–d)), suggesting that PMNZT60/40 has reduced the proportion of tetragonal phase and transformed to cubic phase.

Fig. 4 shows SEM fractured surface micrographs of $(1-x)$ PMNZT60/40– x BZN ceramics investigated by SEM technique.

The samples were sintered at 1100 °C. Fig. 4 (a) shows morphology of the PMNPZT60/40 fractured surfaces. The PMN consists of very fine grains, and loose agglomerates. In contrast, according to Moetakef and Nematib [14], PZT powder consists of agglomerates with larger polygon grain. However, when PMN and PZT are mixed into PMNZT60/40 bulk, they have 97.63% theoretical density due to the applied pressure during the sintering process. Fig. 4 (b–e) shows SEM micrographs of $(1-x)$

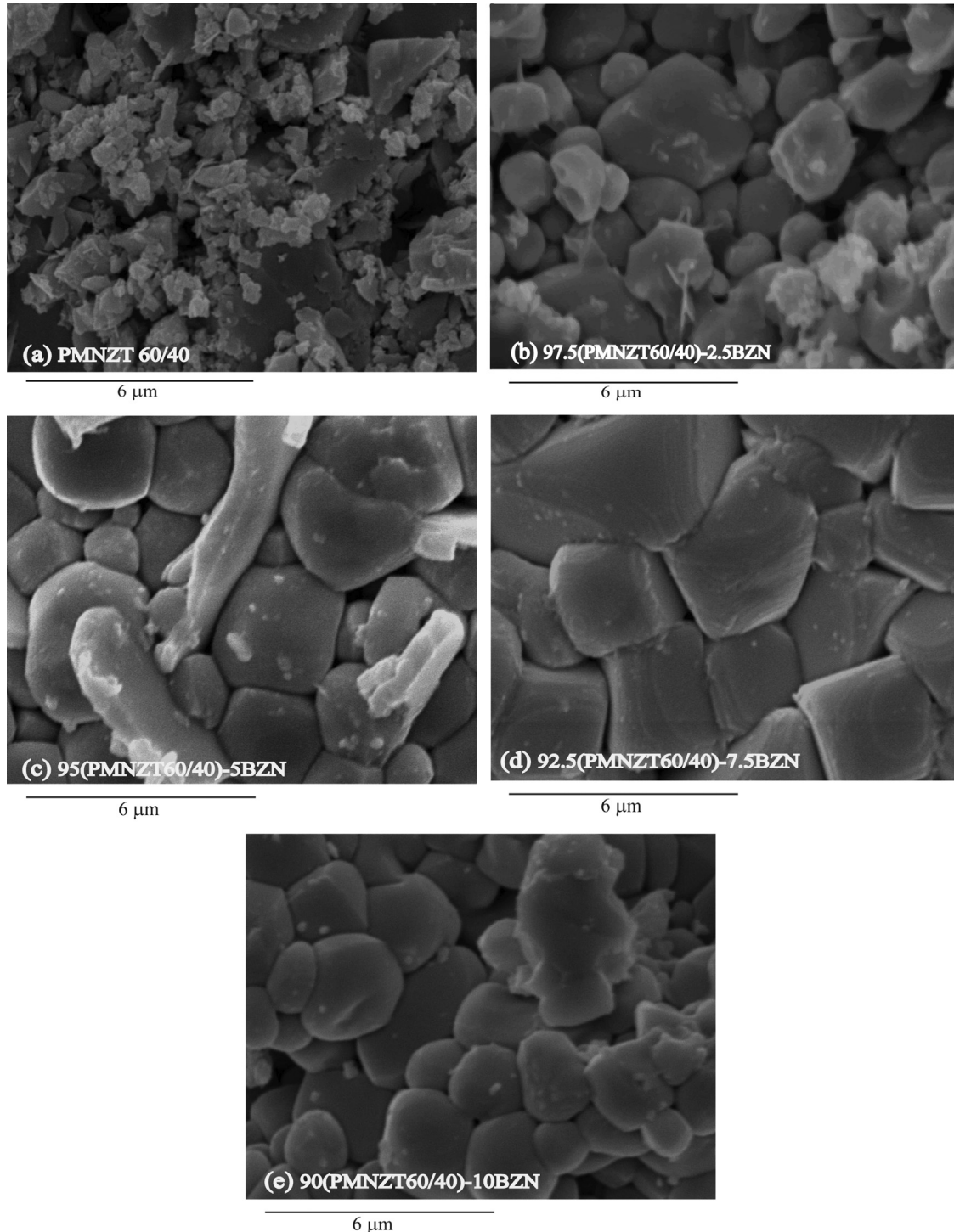


Fig. 4. SEM micrographs from fractured surface of $(1-x)$ PMNZT60/40– x BZN ceramics sintered at 1100 °C while x is equal to (a) 0, (b) 2.5, (c) 5, (d) 7.5, and (e) 10 mol%.

PMN₂T₆₀/40–*x*BZN when *x* = 2.5, 5, 7.5, 10 mol%, respectively. The PMN and BZN composites are agglomerated from fine grains to larger grains due to the larger atomic radius of Pb²⁺ and Ba²⁺ than other atoms, whereas some polygon grains of PZT are also observed. Finally, further addition of BZN (10 mol%) into the composition decreases the density and lowers the grain size [28]. This is believed to result from the sintering temperature for BZN which is higher than that for PMN₂T₆₀/40 [25].

Table 1 displays the percentages of theoretical and experimental densities of sintered (1–*x*)PMN₂T₆₀/40–*x*BZN ceramics. It is noted that the theoretical density slightly decreases with increasing BZN content into PMN₂T₆₀/40. This suggests that either an addition of a large particle size of BZN into the PMN₂T₆₀/40 composition or sintering temperature causes a significant decrease in the density of the bulks [15]. As shown in Table 1, the average grain size of all the mixed compositions is more than the PMN₂T₆₀/40 material. The grain size varies considerably from 1.2 to 2.4 μm. Although, the reason for the changes of the density and the smaller grain sizes could not be clearly indicated in the mixed oxides, but the result implies a BZN role as a grain-growth promoter in the solid state reaction of BZN-modified PMN₂T system [10,15].

3.2. Dielectric properties studies

Dielectric constant as a function of temperature were investigated at various frequencies, as well as the dielectric loss (tan δ) characteristic that consists of a displacement current and conduction current. PMN₂T₆₀/40 ceramic samples added with BZN contents of 0, 2.5, 5, 7.5 and 10 mol% were characterized and the results are shown in Fig. 5 (a–e). In this work, the dielectric properties were measured at frequencies of 1 kHz, 10 kHz and 100 kHz to observe the ferroelectric phase transition behavior and temperature of dielectric maximum (T_{\max}). In the case of PMN₂T₆₀/40 as shown in Fig. 5(a), the dielectric constant (ϵ_r) is found to increase rapidly at temperature 166 °C, suggesting that the phase transition temperature (T_C) occurs at a lower temperature than PMN₂T₅₀/50 [14,15] and then the ϵ_r rapidly decreases, with no frequency dependence. This behavior suggests that PMN₂T₆₀/40 is the normal ferroelectric material, while PMN exhibits the relaxor ferroelectric behavior as a result of a short range ordered structure with heterogeneous in mixed oxide powder [14]. When BZN, a microwave dielectric material, was added to PMN₂T₆₀/40, the dielectric constant was observed to significantly decrease with increasing BZN content. With 2.5 mol% BZN added into PMN₂T₆₀/40, $T_{\max} = 134$ °C is observed, as shown in Fig. 5(b). The dielectric constant as a function of temperature response for dipolar system is shown in Fig. 5(c, d), showing that the BZN contents of 5% and 7.5% mol broadened the peak of dielectric dispersion and T_{\max} at 103 °C and 80 °C, respectively, is observed. This indicates that BZN, the microwave dielectric material, affects the diffused phase transition behavior of PMN₂T materials. The broadening peak of the dielectric constants was found in the compositions with 2.5, 5, 7.5, and 10 mol% BZN addition. The composition with 10 mol% BZN addition shows the dielectric peak at 54 °C, which rapidly decreases with increasing temperature, an indication of the relaxor ferroelectric behavior.

With BZN addition, a similar pattern of low frequency dispersion (LFD) [29] is presented in Fig. 5(b–e). These results clearly suggest that the transition temperature shifts to more of the relaxor behavior with BZN addition.

Comparisons of dielectric properties of PMN₂T–BZN are displayed in Table 2. It is seen that the dielectric properties are comparable to the previous reports on the PMN₂T₅₀/50 and PMN₂T₇₀/30 materials prepared by the composite method. The dielectric constants are high for the composite method and low for the two-step mixed oxide method [14,15]. Dielectric constants of (1–*x*)PMN₂T₆₀/40–*x*BZN when *x* = 0, 2.5, 5, 7.5 and 10 mol% at room temperature are in the range of 1212–4208. With increasing BZN content, the maximum value of the dielectric constant decreases. It should be noted that the grain size increases, while the dielectric constant at temperature of dielectric maximum decreases. It is believed that this porous structure along with inter-cluster exchange mechanism in the Dissado–Hill cluster model for dielectric relaxation [29] and the presence of an amorphous phase are responsible for the low dielectric constants, as compared to other works [30,31].

The dielectric losses are high at higher temperature, as well as high conductivity and correlated dielectric dispersion. Fig. 5(a–e) shows loss tangent (tan δ) of PMN₂T–BZN as a function of temperature. In this case, the temperatures of maximum tan δ are shifted to higher temperature. Furthermore, higher frequency shows abnormality of tan δ. It is noted that increasing frequency introduces high conductivity of activated charges such as Zn²⁺/Nb⁵⁺.

3.3. P–E hysteresis loop studies

Fig. 6 illustrates the polarization–field (*P*–*E*) hysteresis loops of the (1–*x*)PMN₂T₆₀/40–*x*BZN ceramics. The *P*–*E* hysteresis loops indicate that the domain switching behavior of the materials under test. Generally, the *P*–*E* hysteresis loop shape varies greatly with the ferroelectric ceramic composition. For example, PZT shows a well-developed polarization loop and large remnant polarization. The domain switching behavior obtained from *P*–*E* hysteresis loops is usually related to the ferroelectric micro-domain state and a long-range interaction between dipoles, which exhibit a characteristic of a ferroelectric ceramics [10]. In this study, it was found that the largest electric field (before electrical breakdown) applied to the PMN₂T–BZN samples are different for the samples with various BZN contents, which is due to the different electrical resistivity and compositional heterogeneity and porosity of the samples, as seen from the relative density when adding BZN into PMN₂T (Table 1). It should then be noted that in this experiment the constant applied electric field of 10 kV/cm was applied to all the samples due to the limitation explained above. From the *P*–*E* hysteresis loop results (as shown in Fig. 6), the PMN₂T₆₀/40 composition shows a well-developed polarization loop and large remnant polarization, with the maximum remnant polarization P_r and coercive field E_c determined to be 17.5 C/cm² and 5.3 kV/cm, respectively, as listed in Table 3. The hysteresis loop squareness (R_{sq}) is evaluated as one of the ferroelectric properties of the ceramics

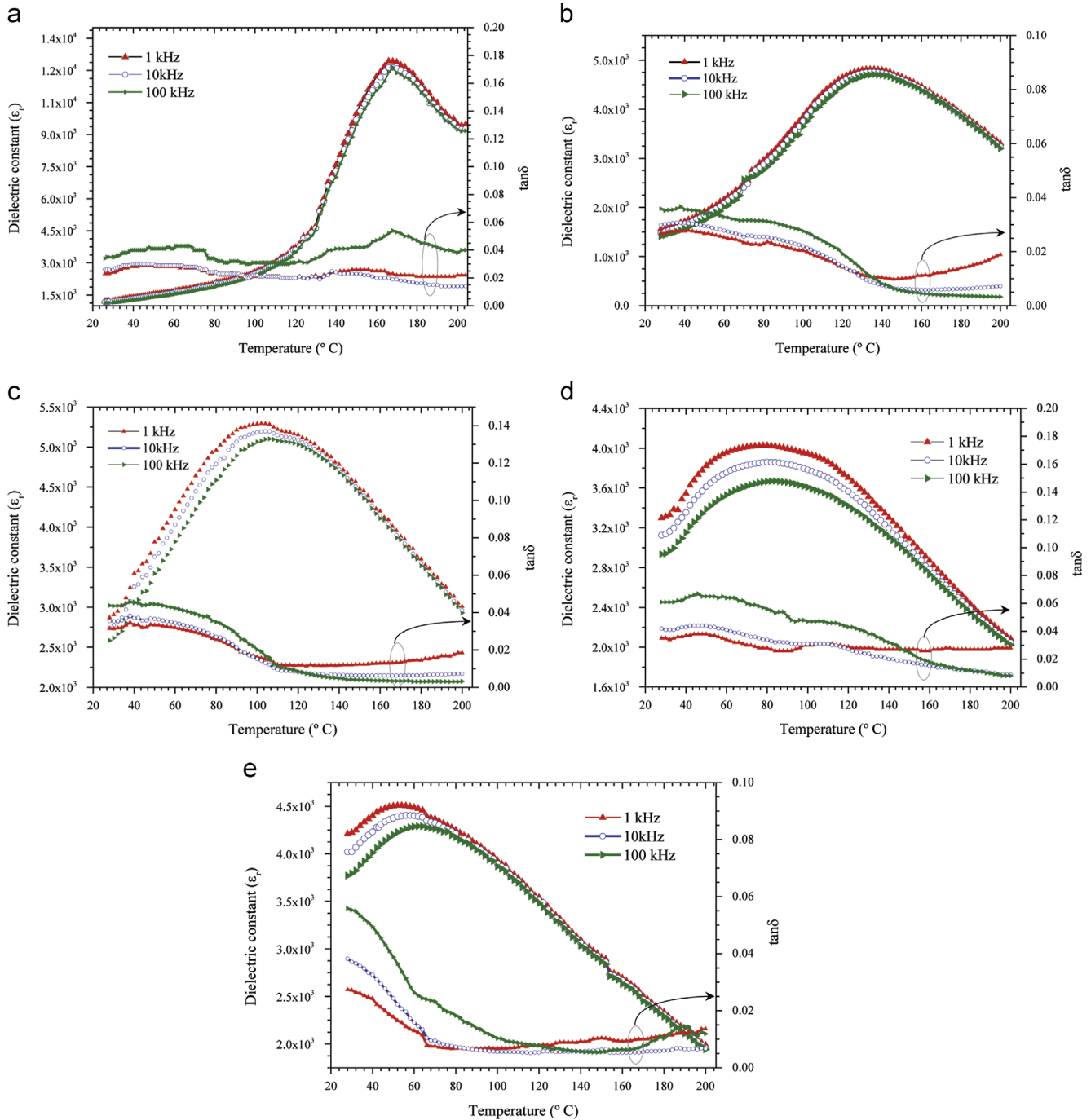


Fig. 5. Temperature and frequency dependences of dielectric properties of (a) PMN₆₀Zn₄₀, (b) 0.975PMN₆₀Zn₄₀–0.025BZN, (c) 0.95PMN₆₀Zn₄₀–0.05BZN, (d) 0.925PMN₆₀Zn₄₀–0.075BZN and (e) 0.9PMN₆₀Zn₄₀–0.1BZN ceramics.

which is the correlation of P_r/P_s . The loop squareness measurement indicates deviation of polarization and electric field with the experimental expression [32].

$$R_{sq} = \frac{P_r^2 + P_{1.1E_C} \cdot P_s}{P_r \cdot P_s} \quad (1)$$

when $P_{1.1E_C}$ is the polarization at $1.1E_C$. For the ideal hysteresis loop defined that R_{sq} as equal to 2.00. Table 3 shows that the R_{sq} decreases from 1.24 for PMN₆₀Zn₄₀ to

0.32 for 0.9PMN₆₀Zn₄₀–0.1BZN. In addition, BZN addition has resulted in the decrease of the values of both P_r and E_C (as listed in Table 3), possibly due to an increased pseudo-cubic phase and more relaxor behavior [7,10]. When more BZN content is added to the $(1-x)$ PMN₆₀Zn₄₀– x BZN system, the P – E hysteresis loops become slim, being a characteristic of the suppressed dipolar interaction [10,33]. This typical activation could be found in the relaxor ferroelectrics with polar switching domain. These results clearly indicate that not only an

Table 2
Dielectric properties of $(1-x)$ PMNZT60/40– x BZN ceramics (1 kHz) at room temperature and temperature of dielectric maximum (T_{\max}).

Samples	Dielectric properties (room temp.)				Dielectric properties (T_{\max})			
	ϵ_r		$\tan \delta$		T_{\max}		$\tan \delta$	
PMNZT 60/40	1212		0.023		12442		0.052	
0.975PMNZT60/40–0.025BZN	1558		0.027		4814		0.012	
0.95PMNZT60/40–0.05BZN	2871		0.032		5292		0.016	
0.925PMNZT60/40–0.075BZN	3298		0.035		4026		0.028	
0.9PMNZT60/40–0.1BZN	4208		0.027		4507		0.016	
	mo.	comp.	mo.	comp.	mo.	com.	mo.	com.
PMNZT 50/50	~693	2200	~0.05	0.04	710	6100	~0.018	0.045
PMNZT 70/30	~1219	5600	~0.015	0.057	1321	10100	~0.035	0.057

mo. is mixed oxide synthesized [14], comp. is composite synthesized [15].

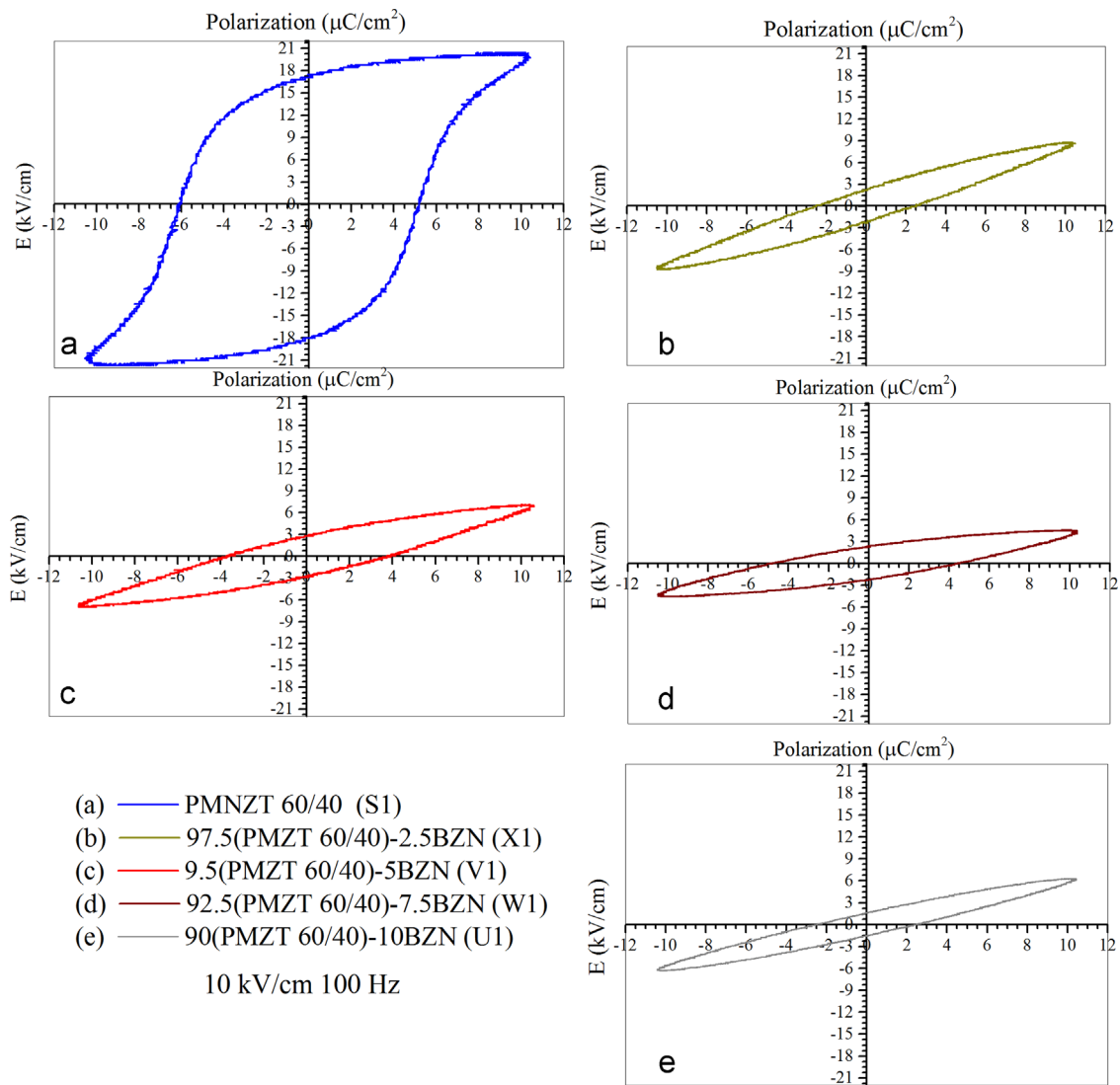


Fig. 6. P - E hysteresis loops of $(1-x)$ PMNZT60/40– x BZN ceramics.

addition of PMN induces the relaxor behavior of PMN into the PMNZT but also the addition of BZN into PMNZT60/40 ceramic system results in more of an electrostrictive behavior in BZN-modified PMNZT system. Thus, more relaxor behavior is induced in PMNZT system with BZN addition.

4. Conclusions

The ceramic compositions of $(1-x)$ PMNZT60/40– x BZN ($x=0, 2.5, 5, 7.5$ and 10 mol%) were prepared from PMNZT added with BZN using the two-step sintering process. Their

Table 3

Parameters from P – E hysteresis loops of $(1-x)$ PMN $Zr_{60/40}$ – x BZN ceramics ($x=0, 2.5, 5, 7.5, \text{ and } 10 \text{ mol\%}$).

Sample	Parameters from P – E hysteresis loops (at 25 °C and applied field of 10 kV/cm)			Loop squareness (R_{sq})
	P_r ($\mu\text{C}/\text{cm}^2$)	P_s ($\mu\text{C}/\text{cm}^2$)	E_C (kV/cm)	
PMN $Zr_{60/40}$	17.5	19.92	5.3	1.24
0.975PMN $Zr_{60/40}$ –0.025BZN	2.33	8.48	2.12	0.39
0.95PMN $Zr_{60/40}$ –0.05BZN	2.79	6.85	3.83	0.52
0.925PMN $Zr_{60/40}$ –0.075BZN	2.4	4.18	4.61	0.80
0.9PMN $Zr_{60/40}$ –0.1BZN	1.86	6.17	2.03	0.32

structural phase transitions were studied in details using X-ray diffraction. With an increase in BZN contents, the structures of the ceramics exhibited a gradual transition process from tetragonal phase to cubic phase, and then transformed to tetragonal when $x=10 \text{ mol\%}$. Crystallite size investigated by TEM technique was in a range of 421–2152 nm. The largest grain size of $(1-x)$ PMN $Zr_{60/40}$ – x BZN was obtained at $x=5 \text{ mol\%}$ and decreased with further increase in BZN contents. The dielectric properties results indicated that the dielectric properties of the PMN $Zr_{60/40}$ followed that of normal ferroelectric, whereas adding BZN into PMN $Zr_{60/40}$ resulted in frequency dispersion and broadening dielectric peaks, an indication of the relaxor behavior. The degree of diffuseness decreased slightly when BZN was added to PMN $Zr_{60/40}$. It was also observed that the transition temperature decreased. The large dielectric constant at room temperature was obtained in the composition with $x=7.5 \text{ mol\%}$ ($\epsilon_r=3298$) and $x=10 \text{ mol\%}$ ($\epsilon_r=4208$). From the P – E hysteresis loops, it was found that for the PMN $Zr_{60/40}$ –BZN system, with BZN addition, more relaxor behavior was induced. When more BZN was added to the $(1-x)$ PMN $Zr_{60/40}$ – x BZN system, the P – E hysteresis loops become slim, showing a characteristic of the suppressed dipolar interaction, found in the relaxor ferroelectrics with polar switching domain. It could then be concluded that more relaxor behavior is induced in PMN $Zr_{60/40}$ system with BZN addition.

References

- [1] R.C. Buchanan, Ceramic Materials for Electronics (revised and expanded), 3rd edition, Marcel Dekker, Inc., 2004.
- [2] A.J. Moulson, J.M. Herbert, Electroceramics, Materials, Properties, Applications, 2nd edition, John Wiley & Sons Ltd., 2003.
- [3] S. Jiansirisomboon, K. Songsiri, A. Watcharapasorn, T. Tunkasiri, Mechanical properties and crack growth behavior in poled ferroelectric PMN–PZT ceramics, Curr. Appl. Phys. 6 (2006) 299–302.
- [4] R. Tipakontitkul, S. Ananta, R. Yimnirun, Phase formation and transitions in the lead magnesium niobate–lead zirconate titanate system, Curr. Appl. Phys. 6 (2006) 307–311.
- [5] H. Ouchi, K. Nagano, S. Hayakawa, Piezoelectric properties of $\text{Pb}(\text{Mg}_{1/3}\text{Nb}_{2/3})\text{O}_3$ – PbTiO_3 – PbZrO_3 solid solution ceramics, J. Am. Ceram. Soc. 48 (1965) 630–635.
- [6] H. Ouchi, Piezoelectric properties and phase relations of $\text{Pb}(\text{Mg}_{1/3}\text{Nb}_{2/3})\text{O}_3$ – PbTiO_3 – PbZrO_3 ceramics with barium or strontium substitutions, J. Am. Ceram. Soc. 51 (1968) 169–176.
- [7] R. Yimnirun, S. Ananta, E. Meechoowas, S. Wongsanmai, Effect of uniaxial stress on dielectric properties of lead magnesium niobate–lead zirconate titanate ceramics, J. Phys. D: Appl. Phys. 36 (2003) 1615–1619.
- [8] T.R. Shrout, A. Halliyal, Preparation of lead-based ferroelectric relaxors for capacitor, Am. Ceram. Soc. Bull. 66 (4) (1987) 704–711.
- [9] A. Halliyal, U. Kumar, R.E. Newnham, L.E. Cross, Stabilization of the perovskite phase and dielectric properties of ceramics in the $\text{Pb}(\text{Zn}_{1/3}\text{Nb}_{2/3})\text{O}_3$ – BaTiO_3 system, Am. Ceram. Soc. Bull. 66 (1987) 671–676.
- [10] V. Koval, C. Alemany, J. Briancin, H. Brunckova, K. Saks, Effect of PMN modification on structure and electrical response of x PMN– $(1-x)$ PZT ceramic systems, J. Eur. Ceram. Soc. 23 (2003) 1157–1166.
- [11] A.V. Shilnikov, A.V. Sopot, A.I. Burkanov, A.G. Luchaninov, The dielectric response of electrostrictive $(1-x)$ PMN– x PZT ceramics, J. Eur. Ceram. Soc. 19 (1999) 1295–1297.
- [12] A.I. Burkanov, A.V. Shilnikov, A.V. Sopot, A.G. Luchaninov, Dielectric and electromechanical properties of $(1-x)$ PMN– x PZT ferroelectric ceramics, Phys. Solid State 42 (2000) 936–943.
- [13] J.C. Shaw, K.S. Lin, I.N. Lin, Dielectric behavior at morphotropic phase boundary for PMN–PZT ceramics, Scr. Mater. 29 (1993) 981–986.
- [14] P. Moetakef, Z.A. Nematib, Study of microstructure and dielectric properties of PMN–PZT ceramics via a mixed powder method including sol–gel precursor, J. Alloy. Compd. 476 (2009) 791–796.
- [15] R. Yimnirun, S. Ananta, P. Laoratanakulb, Dielectric and ferroelectric properties of lead magnesium niobate–lead zirconate titanate ceramics prepared by mixed-oxide method, J. Eur. Ceram. Soc. 25 (2005) 3235–3242.
- [16] M. Sebastian, Dielectric Materials for Wireless Communication, 1st edition, Elsevier, 2008.
- [17] S.F. Wang, Y.R. Wang, C.Y. Liu, W.S. Hsieh, Microwave dielectric properties of multi-ions $\text{Ba}(\text{Zn},\text{Ta})\text{O}_3$ based perovskite ceramics, Ceram. Int. 38 (2012) 1127–1132.
- [18] H. Hughes, D.M. Iddles, I.M. Reaney, Niobate–based microwave dielectrics suitable for third generation mobile phone base stations, Appl. Phys. Lett. 79 (2001) 2952–2954.
- [19] P. Moetakef, Z.A. Nematib, Synthesis of PMN pyrochlore free ceramics via a modified mixed oxide method, J. Electroceram. 19 (2007) 207–213.
- [20] C. Thanachayanont, V. Yordsri, S. Kijamnajsuk, N. Binhayeeniyi, N. Muensit, Microstructural investigation of sol–gel BZT powders, Mater. Lett. 82 (2012) 205–207.
- [21] Z. Xia, Q. Li, Structural phase transformation and electrical properties of $(0.90-x)\text{Pb}(\text{Mg}_{1/3}\text{Nb}_{2/3})\text{O}_3$ – $x\text{PbTiO}_3$ – $0.10\text{Pb}(\text{Fe}_{1/2}\text{Nb}_{1/2})\text{O}_3$ ferroelectric ceramics near the morphotropic phase boundary, Acta Mater. 55 (2007) 6176–6181.
- [22] Z. Xia, Q. Li, Phase transformation in $(0.90-x)\text{Pb}(\text{Mg}_{1/3}\text{Nb}_{2/3})\text{O}_3$ – $x\text{PbTiO}_3$ – 0.10PbZrO_3 piezoelectric ceramic: X-ray diffraction and Raman investigation, Solid State Commun. 142 (2007) 323–328.
- [23] S.M. Gupta, D. Viehland, Tetragonal to rhombohedral transformation in the lead zirconium titanate lead magnesium niobate lead titanate crystal-line solution, J. Appl. Phys. 83 (1998) 407–414.
- [24] L.L. Hsiung, M.J. Fluss, S.J. Tumeay, B.W. Choi, Y. Serruys, F. Willaime, A. Kimura, Formation mechanism and the role of nanoparticles in Fe–Cr ODS steels developed for radiation tolerance, Phys. Rev. B 82 (2010) 184103.
- [25] D.G. Morris, M.A. Morris, Microstructure and strength of nanocrystalline copper alloy, Acta Metall. Mater. 39 (1991) 1763–1770.
- [26] C. Suryanarayana, E. Ivanov, V.V. Boldyrev, The science and technology of mechanical alloying, Mater. Sci. Eng. A. 304–306 (2001) 151–158.
- [27] D. Brandon, W.D. Kaplan, Microstructural Characterization of Materials, Technion, Israel Institute of Technology, 2nd edition, John Wiley & Sons Ltd., Israel, 2008, p. 224.

- [28] Y.C. Liou, Y.C. Shih, C.J. Chuang, Y.T. Chen, Synthesis and properties of $(\text{Ba}_x\text{Pb}_{1-x})(\text{Zn}_{1/3}\text{Nb}_{2/3})\text{O}_3$ relaxor ferroelectric ceramics using a reaction-sintering process, *Ceram. Int.* 34 (2008) 1413–1418.
- [29] D.K. Dass Gupta, P.C.N. Scarpa, *Electr. Insul.* 15 (1999) 23–32.
- [30] B. Noheda, Structure and high-piezoelectricity in lead oxide solid solutions, *Curr. Opin. Solid State Mater. Sci.* 6 (2002) 27–34.
- [31] S.K. Mishra, D. Pandey, A.P. Singh, Effect of phase coexistence at morphotropic phase boundary on the properties of $\text{Pb}(\text{Zr}_x\text{Ti}_{1-x})\text{O}_3$ ceramics, *Appl. Phys. Lett.* 69 (1996) 1707–1709.
- [32] B.M. Jin, J. Kim, S.C. Kim, Effects of grain size on the electrical properties of $\text{PbZr}_{0.52}\text{Ti}_{0.48}\text{O}_3$ ceramics, *Appl. Phys.* 65 (1997) 53–56.
- [33] V. Koval, C. Alemany, J. Briancin, H. Brunckova, Dielectric properties and phase transition behavior of $(x)\text{PMN}-(1-x)\text{PZT}$ ceramic systems, *J. Electroceram.* 10 (2003) 19–29.